Uniosun Journal of Engineering and Environmental Sciences (UJEES), Vol. 8 No. 2, Sept., 2026
DOI: 10.64980/ujees.v8i2.011 **Oyedele et al.**
Published: September 30, 2026

COMPARATIVE ANALYSIS OF METAHEURISTIC OPTIMIZERS FOR OPTIMAL THYRISTOR-CONTROLLED SERIES CAPACITOR SITING AND SIZING IN THE NIGERIAN 28-BUS TRANSMISSION NETWORK

Olusola Joel OYEDELE [1*], Ganiyu Adedayo AJENIKOKO [2], Isaiah Gbadegesin ADEBAYO [3] and Abdulbasit Adedayo AJENIKOKO [4]

[1]Electrical and Electronic Engineering, Bowen University Iwo, Osun State, Nigeria
[2,3]Electronic and Electrical Engineering, Ladoke Akintola University of Technology, Ogbomoso, Oyo State, Nigeria
[4]Electrical and Electronics Engineering, The Federal Polytechnic Ayede, Ogbomoso, Nigeria

[*]Corresponding Author: olusola.oyedele@bowen.edu.ng

Abstract
The Nigerian 330-kV transmission network exhibits poor voltage profiles and localized voltage instability associated with long radial feeders, limited reactive reserves, and generation–load mismatch, motivating coordinated Thyristor-Controlled Series Capacitor (TCSC) siting and sizing. However, the combined use of voltage-stability-based candidate screening, comparative metaheuristic optimization, and N−1 robustness assessment that distinguishes electrical from structural criticality remains insufficiently addressed for the Nigerian 28-bus network. A framework comprising Newton–Raphson load flow, Fast Voltage Stability Index (FVSI) screening, and a common weighted objective function for Political Optimizer (PO), Doctor and Patient Optimizer (DPO), and Ant Colony Optimization (ACO) was implemented on the 28-bus, 330-kV system. The five highest-FVSI lines were screened as candidate locations, while 20 independent runs with matched population and iteration budgets enabled repeatability assessment; N−1 analysis was subsequently applied to the eight most critical lines. All three algorithms identified Line 1–20 with a compensation degree of (k_c=-0.6771), corresponding to a 67.7% reduction in line reactance. DPO and ACO reproduced this solution in all 20 runs, whereas PO achieved it in 13 runs. The optimized TCSC reduced the sum-of-squared voltage deviation by 53.9% and RMS VDI by 32.1%, increasing the minimum voltage from 0.9379 to 0.9751 p.u.; however, active losses increased by 18.0%, from 925.78 to 1092.04 MW. Under survivable N−1 contingencies, VDI improved in all three cases, while losses increased in two. The results demonstrate that FVSI effectively screens stressed lines. The optimal compensation siting highlights the need for optimization-based FACTS planning and explicit structural-contingency assessment in sparsely meshed transmission networks.

Keywords
Voltage stability, TCSC, FACTS, Political Optimizer, Doctor and Patient Optimizer, Ant Colony Optimization, Fast Voltage Stability Index, N-1 contingency analysis, Nigeria 330 kV network

1. INTRODUCTION

The Nigerian 330 kV transmission grid has, over the past decade, experienced recurring poor voltage profiles, high transmission losses, and localized voltage instability, driven by long radial feeders, insufficient reactive power reserves, and a generation-load geographic mismatch [1]. Voltage instability has led to repeated voltage collapse and cascading outages, with severe economic and social consequences [2]. Flexible AC Transmission System (FACTS) devices, and in particular series-connected compensators such as the Thyristor-Controlled Series Capacitor (TCSC), have become an established tool for improving voltage profiles, increasing power transfer capability, and mitigating loop flows on stressed corridors [3]. The effectiveness of TCSC deployment is largely determined by two interlinked aspects: where in the grid network to deploy the device and what amount of series compensation to apply [4]. Both are combinatorial, non-convex problems that are increasingly solved using metaheuristic optimization rather than existing analytical methods [5]. A wide range of nature- and society-inspired algorithms have been proposed for FACTS siting and sizing problems in the literature; however, comparative studies that rigorously benchmark algorithms, such as the Political Optimizer and the Doctor and Patient Optimizer, against more established approaches like Ant Colony Optimization, specifically for TCSC placement on a practical Nigerian network,

remain limited. TCSC was selected over shunt FACTS devices such as SVC or STATCOM, and over the more complex UPFC, because the target congestion and stress pattern identified by FVSI screening is line-based rather than bus-based. The stressed elements are transmission lines carrying disproportionate power relative to their thermal/stability limit. Also, not all buses need direct local reactive support. A series device controls the impedance of the network, and hence the power flow through the stressed line, redistributing loading and reducing system losses; a shunt device (SVC/STATCOM) would instead inject reactive power at a bus and is the more appropriate choice where the problem is localized bus-voltage depression rather than line congestion. Any voltage-profile improvement reported in this study is therefore a secondary consequence of loss and flow redistribution, not direct bus voltage support, and is described accordingly throughout. This paper makes the following contributions: Application of the Fast Voltage Stability Index (FVSI) to screen TCSC candidate lines on the Nigeria 28-bus 330 kV network from a base-case Newton-Raphson power flow, A shared weighted objective function used to evaluate PO, DPO, and ACO across identical candidate transmission lines. A cross-validated comparison of convergence speed and solution quality for TCSC siting and sizing, in which independent agreement across three structurally different algorithms is used as corroborating evidence for the optimum found. An N-1 single-line contingency robustness study of the best-found TCSC placement, including a structural screening step that distinguishes electrically critical lines from lines whose outage disconnects part of the network outright, which is an assessment frequently omitted from FACTS siting studies but essential for practical deployment. The remainder of this paper is organized as follows. Section 2 reviews related work on voltage stability indices and metaheuristic FACTS placement. Section 3 details the methodology, including the test system, power-flow formulation, TCSC model, FVSI screening procedure, three optimisation algorithms, and the N-1 contingency framework. Section 4 presents and discusses the results. Section 5 concludes the paper and outlines directions for future work. Numerous indices have been proposed to quantify a power system's proximity to voltage collapse and identify weak buses or branches that require reactive power support. Line-based indices such as the Fast Voltage Stability Index (FVSI) [6], the Line Stability Index (Lmn) [7], and the Line Stability Factor (LQP) [8] evaluate stress on individual transmission lines from a single power flow, while bus-based indices such as the L-Index and the Voltage Collapse Proximity Index (VCPI) rank load buses by their electrical distance from collapse [9]. Adebayo and Sun [10] proposed the Voltage Collapse Critical Bus Index (VCCBI), which instead subjects each load bus to incremental reactive power stress and tracks the cumulative voltage deviation until the power flow diverges, normalizing by the number of steps survived and the maximum reactive loadability reached; related work by Adebayo et al. [11] analyzed voltage collapse using a comparable family of indices. This study adopts the line-based FVSI, detailed in Section 3.4, to screen TCSC candidate lines on the Nigeria 28-bus system, because a series compensator is placed on a line rather than at a bus, making a line-based screening index the more directly applicable choice. FACTS device siting and sizing is typically formulated as a mixed discrete-continuous, non-convex optimization problem and solved using metaheuristics such as Genetic Algorithms [12], Particle Swarm Optimization [13], Grey Wolf Optimizer [14], and various hybrid schemes. Ant Colony Optimization, in its continuous form [15], has been widely applied to power system optimization problems owing to its archive-based, Gaussian-kernel sampling mechanism, which balances exploration and exploitation without requiring gradient information. More recently, socio- and process-inspired metaheuristics such as the Political Optimizer [16], which models multi-party election dynamics, and the Doctor and Patient Optimizer, which models treatment-based interactions between candidate solutions, have shown competitive performance on general optimization benchmarks, but their application to FACTS device siting on Nigerian transmission networks and comparative benchmarking against ACO in particular has not been extensively reported. While voltage-stability-index-based FACTS placement and metaheuristic FACTS sizing have each been studied extensively in isolation, a combined FVSI-screened, multi-algorithm comparative study of TCSC placement and inclusive of N-1 contingency robustness testing, that distinguishes electrical criticality from structural (topological) criticality. A review of the literature identified limited studies that combine FVSI-screened, multi-algorithm comparative TCSC placement with N-1 contingency robustness testing distinguishing electrical from structural criticality for the Nigeria 28-bus 330 kV network.

2. MATERIALS AND METHOD

2.1 Test System Description

The study is conducted on the Nigeria 28-bus 330 kV transmission network, comprising 28 buses (1 slack, 9 PV/generator buses, and 18 PQ/load buses) and 31 transmission branches, with a system MVA base of 100 MVA and a voltage base of 330 kV [17]. Bus data (voltage setpoints, active and reactive loads, generation limits) and line data (series resistance, series reactance, half-line charging susceptance, and tap ratio) were obtained from the source network dataset [18]. The network is sparsely meshed: 31 branches serve 28 buses, only four branches more than the 27 required for a bare spanning tree. This low level of redundancy is consequential for the N-1 contingency analysis reported in Section 4.7, where several of the most electrically stressed lines are also topological bridges whose removal would disconnect part of the network.

2.2 Power Flow Formulation

The base-case and all subsequent (TCSC-modified and contingency) operating points are solved using the standard polar-coordinate Newton-Raphson iterative method. The active and reactive power injections at bus i are [19], [20]:

$$P_i = \sum_{j=1}^{N} V_i V_j \left(G_{ij} \cos\left(\delta_i - \delta_j\right) + B_{ij} \sin\left(\delta_i - \delta_j\right)\right) \quad (1)$$

$$Q_i = \sum_{j=1}^{N} V_i V_j \left(G_{ij} \sin\left(\delta_i - \delta_j\right) - B_{ij} \cos\left(\delta_i - \delta_j\right)\right) \quad (2)$$

where V_i, δ_i are the voltage magnitude and angle at bus i, and G_{ij}, B_{ij} are the conductance and susceptance (real and imaginary parts, respectively) of the bus admittance matrix Y_bus. Defining the specified and calculated injections at bus i as P_i, spec/Q_i, spec and P_i, calc/Q_i,calc (Eqs. 1-2), the power-mismatch equations solved at each iteration are $\Delta P_i = P_i,\text{spec} - P_i,\text{calc}(V,\delta)$ and $\Delta Q_i = Q_i,\text{spec} - Q_i,\text{calc}(V,\delta)$ for all PQ and PV buses. These mismatch vectors are linearized via the Jacobian matrix and solved iteratively to a tolerance of 1×10^{-6} per unit [21], [22].

2.3 TCSC Steady-State Model

The fundamental-frequency, firing-angle-based TCSC steady-state model (impedance-control formulation with no droop) provides the underlying physical basis for TCSC series reactance control:

$$P + V_k V_m B_e sine(\delta_k - \delta_m) = 0 \quad (4)$$

$$-V_k^2 B_e + V_k V_m B_e \cos(\delta_k - \delta_m) - Q_k = 0 \quad (5)$$

$$-V_m^2 B_e + V_k V_m B_e \cos(\delta_k - \delta_m) - Q_m = 0 \quad (6)$$

$$B_e - B_e(\alpha) = 0 \quad (7)$$

$$\sqrt{(P^2 + Q_k^2)} - IV_k = 0 \quad (8)$$

where B_e is the series susceptance of the TCSC, V_k and V_m are the terminal voltages of the controller, δ_k and δ_m are the terminal angles, Q_k and Q_m are the reactive power injections at the two terminals, and P and I are the active power and current through the controller. $B_e(\alpha)$ is a nonlinear function of the thyristor firing angle α [21].

Solving Equations (4)–(8) for α at every fitness evaluation of every candidate solution (potentially tens of thousands of evaluations per optimization run; Section 3.10) is computationally prohibitive for a metaheuristic search loop. This study therefore implements the equivalent variable-series-reactance representation of the TCSC that is commonly used in FACTS siting/sizing optimization studies: the compensated line's series reactance is scaled directly by a compensation degree kc,

$$X_line,new = X_line,original \times (1 + kc) \quad (9)$$

where $kc \in [-0.7, 0.2]$ is the decision variable sized by each metaheuristic; negative kc denotes capacitive compensation (reduces reactance), positive kc denotes inductive compensation (increases reactance).

This sign convention and bound are the standard ones used in the TCSC siting/sizing optimization (Shokouhandeh et al. [23], which give

$$X = X_line + X_TCSC = (1 + r)X_line$$

with r bounded to $[-0.8, 0.2]$ and negative r denoting capacitive (reactance-reducing) mode. Bansal et al. [24] independently report a working range of $-0.7 \cdot X_line$ to $0.2 \cdot X_line$ for the same compensation coefficient; both bounds trace to the practical thyristor-rating limits discussed in Hingorani and Gyugyi [25].

This modified reactance is substituted directly into the corresponding row of the line-data matrix before each Newton-Raphson power-flow solve, so the TCSC's effect on line loading, system losses, and bus voltages is captured self-consistently at every fitness evaluation, without needing to resolve the internal firing-angle relationship (Eqs. 4–8) at each step.

Line thermal ratings were not available for this dataset; the reported TCSC size is therefore expressed in reactance terms (Ω, % of line reactance) rather than MVAr, consistent with standard practice in FACTS siting/sizing studies where device ratings are typically expressed relative to line impedance.

2.4 Fast Voltage Stability Index (FVSI)

For each transmission line connecting a sending bus i and receiving bus j, the Fast Voltage Stability Index is computed from the base-case power flow solution as [26]:

$$FVSI_{ij} = \frac{4|Z_{ij}|^2 Q_r}{V_s^2 X_{ij}} \quad (15)$$

where Z_{ij} and X_{ij} are the series impedance and reactance of the line, Q_j is the reactive power received at the far end of the line, and V_i is the sending-end voltage magnitude. An FVSI value near 1.0 indicates that the power line is near its voltage-collapse limit. Lines are ranked in descending order of FVSI, and the five highest-ranked lines form the candidate set for TCSC placement.

2.5 Voltage Deviation Index

The Voltage Deviation Index (VDI) evaluates the total grid voltage deviation from the nominal reference value ($V_{\text{ref}} = 1.0$ pu) across all 28 buses using three standard power system formulations [27], [28], [29]:

a. Sum of Squared Deviations ($\text{VD}_{\text{squared}}$):

$$VD_{\text{squared}} = \sum_{i=1}^{28}(V_i - 1.0)^2 \quad (16)$$

b. Sum of Absolute Deviations ($\text{VD}_{\text{absolute}}$):

$$VD_{\text{absolute}} = \sum_{i=1}^{28} |V_i - 1.0| \quad (17)$$

c. Root Mean Square Index (VDI_{RMS}):

$$VDI_{\text{RMS}} = \sqrt{\frac{1}{28}\sum_{i=1}^{28}(V_i - 1.0)^2} \quad (18)$$

2.6 Objective Function

All three algorithms optimize the same two-dimensional decision vector x = [line selector, kc] over the FVSI-screened candidate line set, minimizing the composite fitness:

$$F(x) = w_1\left(\frac{P_{loss}}{P_{loss,base}}\right) + w_2 \cdot VDI \quad (19)$$

where P_loss is the total system active power loss with the TCSC applied, P_loss, base is the base-case loss, and VDI is the sum-of-squared-deviations voltage index across all buses (Section 4.6). Weights $w_1 = 0.5$ and $w_2 = 0.5$ were used to balance loss minimisation against voltage-quality objectives, applied identically across PO, DPO, and ACO to ensure a comparison. A formal sensitivity analysis of these weights is left for future work. The optimization is subject to: (i) the line selector being restricted to the discrete set of FVSI-screened candidate lines (ii) kc ∈ [−0.7, 0.2]; (iii) the TCSC power-flow equality constraints, Equations (4), (5), (7) and (8), being satisfied at every fitness evaluation; and (iv) bus voltage magnitudes remaining within the [0.90, 1.05] p.u. operating band (Table 1), enforced through the VDI term of the fitness function.

2.7 Political Optimizer

The PO process is modelled in Equations (20)–(26) [30], using distinct notation for population size parameters to avoid ambiguity: Np is the number of political parties (N_p = 5 in this study), Nc is the number of electoral constituencies, and d is the number of decision-variable dimensions (d = 2: the FVSI-screened line index and kc).

The entire population is divided into Np political parties:

$$\text{P} = \{\text{P}_1, \text{P}_2, \ldots, \text{P_\{Np\}}\} \quad (20)$$

Each party fields one candidate per constituency, giving Nc members per party:

$$\text{P}_\text{i} = \{\text{p}_\text{i}^{\,1}, \text{p}_\text{i}^{\,2}, \ldots, \text{p}_\text{i}\text{\^\{N_c\}}\} \quad (21)$$

Each party member is a d-dimensional solution vector:

$$\text{p}_\text{i}^{\,\text{j}} = [\text{p}_{\text{i},\,1}^{\,\text{j}}, \text{p}_{\text{i},\,2}^{\,\text{j}}, \ldots, \text{p}_{\text{i},\,\text{d}}^{\,\text{j}}]^{\text{T}} \quad (22)$$

The same population is also partitioned into Nc electoral constituencies [31]:

$$\text{C} = \{\text{C}_1, \text{C}_2, \ldots, \text{C_\{Nc\}}\} \quad (23)$$

Each constituency contains one member from every party, i.e. Np members:

$$\text{C}_\text{j} = \{\text{p}_1^{\,\text{j}}, \text{p}_2^{\,\text{j}}, \ldots, \text{p_\{Np\}}^{\text{j}}\} \quad (24)$$

The party leader is the member with the best fitness in that party:

$$\text{q} = \arg\min_{1 \le \text{j} \le \text{Nc}} \text{f}(\text{p}_\text{i}^{\,\text{j}}), \forall \text{i} \in \{1, \ldots, \text{N_p}\};\ \ \text{p}_\text{i}* = \text{p}_\text{i}^{\,\text{g}} \quad (25)$$

All party leaders together form:

$$\text{P}* = \{\text{p}_1*, \text{p}_2*, \ldots, \text{p_\{N_p\}}*\} \quad (26)$$

The continuous line-selector coordinate returned by each algorithm is mapped to a discrete FVSI-candidate line index by rounding to the nearest integer and clamping to the valid range [1, n_candidates] before being used to index into the candidate-line table; the same discretization rule is applied identically inside the shared objective function for PO, DPO, and ACO, so all three algorithms search the same effective discrete-continuous space.

2.8 Doctor and Patient Optimizer

The Doctor and Patient Optimizer (DPO) implemented here uses a population of N = 50 "patients" and two update phases per iteration, applied to each patient independently with equal probability:

Treatment phase (selected with probability 0.5): the patient moves toward the best-so-far solution (the "doctor"),

$$\text{x_new} = \text{x_i} + \text{a} \cdot \text{r}_1 \cdot (\text{x_doctor} - \text{x_i}) \quad (27)$$

Surgery phase (selected with probability 0.5): a more exploratory update using a randomly chosen other patient $j \neq i$,

$$x_new = x_doctor + (2r_2 - 1) \cdot a \cdot (x_j - x_i) \quad (28)$$

In both phases, r_1 and r_2 are independent uniform random numbers on [0,1], and $a = 2 - 2(iter/iter_max)$ is a linearly decreasing treatment-intensity factor that shifts the search from exploration in early iterations to exploitation in later ones. Each patient's update is accepted only if it improves that patient's own fitness (greedy selection); the doctor is updated whenever any patient in the population achieves a new best fitness. This two-phase structure (Treatment/Surgery) is the one actually implemented and evaluated in this study; it is a simplified variant of the broader family of DPO algorithms in the metaheuristics literature [32], some of which define three or more phases.

2.9 Ant Colony Optimizer (ACO)

An Ant Colony Optimizer is used to maintain a solution archive ranked by fitness [15]. New candidate solutions ("ants") are sampled from a Gaussian kernel probability density function constructed from the archive, with the guiding archive member selected via rank-weighted roulette selection and the sampling standard deviation at each dimension derived from the mean pairwise distance among archive members, scaled by a locality parameter $q = 0.1$ and a convergence-rate parameter $\xi = 0.85$. The archive size is 20, and $N = 50$ ants are generated per iteration (matching the PO/DPO population size).

The rank-based selection weight for archive member r (rank 1 = best) is

$$w_r = 1/(q \cdot k \cdot \sqrt{(2\pi)}) \cdot \exp(-(r-1)^2 / (2q^2k^2)) \quad (29)$$

with $k = 20$, the archive size, normalized to a selection probability $p_r = w_r / \Sigma w_r$. Out-of-bound samples are clamped to [lb, ub]. The archive is elitist: at each iteration, the best solutions among the merged archive and newly sampled ants are retained. Figure 2 is a block diagram for the ACO employed in this work.

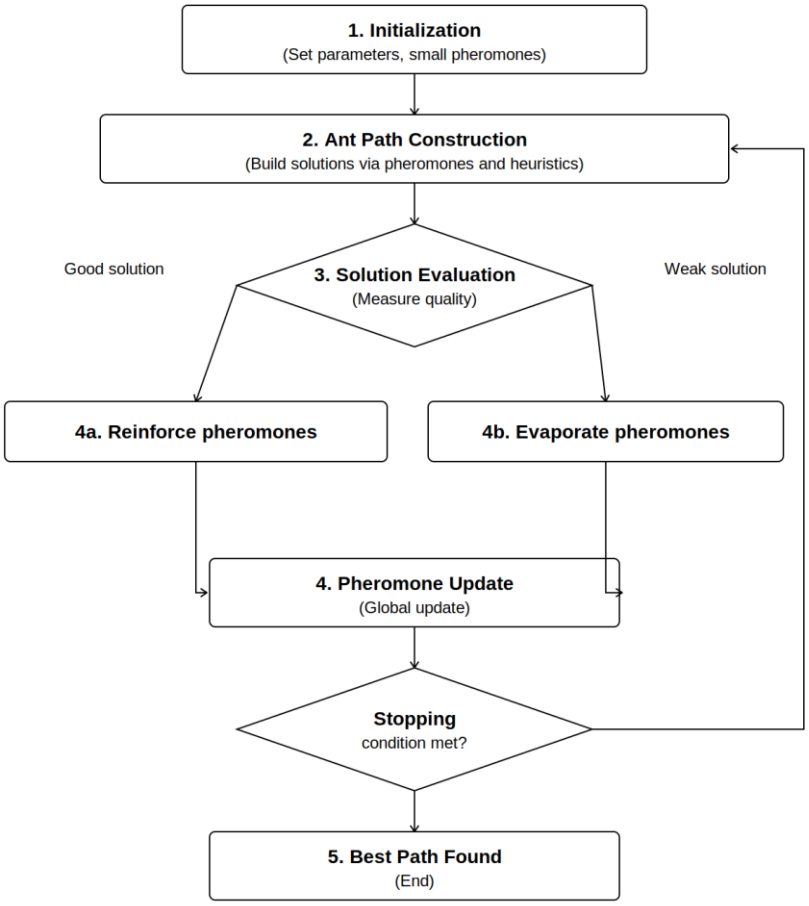


Figure 1. Ant Colony Optimization (ACO) Algorithm Flowchart

2.10 Experimental Setup

Table 1. Experimental setup shared across PO, DPO, and ACO.

Parameter	Value
Population size	50 (5 parties × 10 constituencies for PO; matched for DPO/ACO)
Maximum iterations	15
Independent trials per algorithm	20
TCSC compensation bound (kc)	−0.7 to 0.2
Voltage limits	0.90–1.05 p.u. (penalty band); 0.95–1.05 p.u. (target)
Objective weights (w_1, w_2)	0.5, 0.5

All three algorithms were run with matched population size and iterations to ensure a fair comparison.

2.11 N-1 Contingency Analysis Framework

To assess the robustness of the best-found TCSC placement, the top eight FVSI-ranked lines are selected as an N-1 contingency set. For each contingency, network connectivity from the slack bus is first checked by first search on the post-outage topology and contingencies. The ones that disconnect one or more buses from the slack are classified as critical and excluded from load-flow-based comparison. Since no power-flow solution exists, part of the network has no path back to the reference bus. For the remaining survivable contingencies, the power flow is re-solved twice: once without the TCSC and once with the TCSC installed at its optimized location and compensation level. For each case, total active power loss, the voltage deviation index, and the minimum bus voltage are recorded and compared [33].

3. RESULTS AND DISCUSSION

3.1 Base Case Load Flow Results

The Newton-Raphson power flow converged in 5 iterations. Total system generation was $2886.78\ \text{MW}/624.08\ \text{MVAr}$ against a load of $1961.00\ \text{MW}/1462.82\ \text{MVAr}$, yielding total active losses of $925.78\ \text{MW}$ and reactive losses of $-838.74\ \text{MVAr}$. The base-case voltage profile yielded $VD_{\text{squared}} = 0.0129$, $VD_{\text{absolute}} = 0.3793$, and $VDI_{\text{RMS}} = 0.0214$, with the minimum voltage of $0.9379\ \text{p.u.}$ occurring at Bus 19. Table 2 reports the full bus voltage profile (Base Case Results of the Nigeria 28-Bus System).

Table 2: Base case results of the Nigeria 28-Bus system

No	Type	Voltage Magnitude (pu)	Phase Angle/degree
Bus 1	Swing	1.0000	0.0000
Bus 2	PV	1.0000	20.3720
Bus 3	PV	1.0000	16.4270
Bus 4	PV	1.0000	18.5000
Bus 5	PV	1.0000	15.5090
Bus 6	PV	1.0000	16.5330
Bus 7	PV	1.0000	37.2490
Bus 8	PV	1.0000	0.0735
Bus 9	PV	1.0000	28.0400
Bus 10	PV	1.0000	46.2550
Bus 11	PQ	1.0242	13.8830
Bus 12	PQ	0.9994	16.4010
Bus 13	PQ	1.0221	14.0230
Bus 14	PQ	0.9895	18.0690
Bus 15	PQ	0.9617	8.5616
Bus 16	PQ	0.9803	10.8150
Bus 17	PQ	1.0160	13.9600
Bus 18	PQ	1.0167	13.1530
Bus 19	PQ	0.9379	5.8568
Bus 20	PQ	0.9431	6.3286
Bus 21	PQ	0.9759	26.4180

Bus 22	PQ	0.9772	29.7880
Bus 23	PQ	0.9861	36.5970
Bus 24	PQ	0.9995	17.8780
Bus 25	PQ	0.9948	-0.3304
Bus 26	PQ	1.0055	14.6160
Bus 27	PQ	1.0157	16.5780
Bus 28	PQ	1.0246	16.2170

3.2 Stability Index Ranking and Candidate Lines

Evaluating the Fast Voltage Stability Index ($FVSI$) across all transmission lines (31) yielded the stress ranking presented in Table 3. Line 21–23 ($FVSI = 0.80147$) and Line 17–20 ($FVSI = 0.75747$) were identified as the most heavily stressed interconnecting corridors. The top 5 ranked lines were selected as candidate branches for TCSC siting and sizing by metaheuristic optimization.

Table 3: Top 10 FVSI-ranked lines with values.

Rank	Line (From–To)	FVSI
Rank 1	**21–23**	**0.8015**
Rank 2	**17–20**	**0.7575**
Rank 3	**10–23**	**0.7108**
Rank 4	**17–21**	**0.322**
Rank 5	**1–20**	**0.3077**
Rank 6	16–17	0.1863
Rank 7	3–26	0.1493
Rank 8	27–28	0.0878
Rank 9	3–17	0.0872
Rank 10	4–27	0.0869

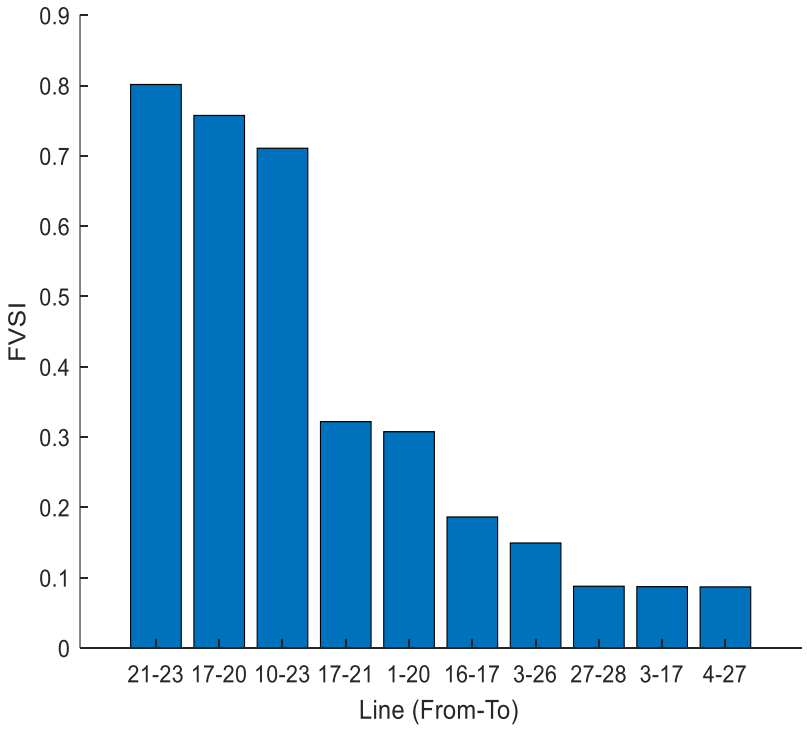


Figure 2. Top 10 FVSI-ranked lines (base case).

Efficacy of FVSI Candidate Screening and Baseline Dispatch Nuances.
Lines 21-23, 17-20, and 10-23 were identified as the top three stressed branches by FVSI. The optimisation procedures, however, converged not on any of these three but on the lowest-ranked candidate, Line 1–20 (FVSI rank 5 of 5). This is a striking demonstration that the line most electrically stressed by FVSI's line-based criterion is not necessarily the most effective site for series compensation once the actual power-flow and voltage-deviation objective is evaluated directly. One important factor in the analysis of the results is the base-case operating dispatch. The loss-to-load ratio determined by the base-case Newton-Raphson load flow was about 47% (925.78 MW loss against 1961.00 MW load). All metaheuristic models (PO, DPO, ACO) were tested on the same base-case power-flow model.
To verify this directly, the objective function was evaluated at its own best-found kc for each of the five FVSI-screened candidate lines individually (grid search over $kc \in [-0.7, 0.2]$ in steps of 0.01), rather than relying only on the line's result:

Table 4: Best achievable objective value for each FVSI-screened candidate line.

Candidate	Line (From–To)	FVSI Rank	Best kc	Best Objective F(x)
1	21–23	1 (highest FVSI)	0.2000	0.989856
2	17–20	2	0.2000	0.945783
3	10–23	3	0.2000	0.997073
4	17–21	4	−0.5300	0.981885
5	1–20	5 (lowest FVSI)	−0.6800	0.820212

Line 1–20 (Candidate 5) achieves the lowest value, which implies that the best objective value (0.8202) of all five candidates. A comprehensive assessment establishes the convergence on Line 1–20 as the global minimum of the objective function, thereby excluding any potential false minimum created by the algorithm or a premature stochastic trap. Other candidates, apart from the three topmost FVSI branches, showed poor performance, with values ranging between 0.92 and 1.00. This directly supports the paper's claim that FVSI rank alone does not determine the best TCSC site: the least electrically stressed of the five candidates is in fact the most effective compensation point once the actual loss/voltage trade-off is evaluated.

3.3 Optimization Results per Algorithm

Table 5 summarizes the best TCSC placement and sizing found by each algorithm within the shared evaluation budget (Table 1). It is worth mentioning that the line between Buses 1 and 20, the lowest-ranked of the five FVSI-screened candidates, was chosen as the optimal TCSC placement by all three algorithms considered — not the highest-FVSI line, underscoring that FVSI screening identifies candidates for evaluation, not the final answer. PO, DPO, and ACO all found the same compensation value in their best runs, kc = −0.6771.

Table 5a: Best TCSC siting and sizing result per algorithm.

Quantity	Base Case	PO-Sized TCSC	DPO-Sized TCSC	ACO-Sized TCSC
TCSC Location	—	Line 1–20	Line 1–20	Line 1–20
Compensation Degree (kc)	—	−0.6771	−0.6771	−0.6771
Physical TCSC Size |ΔX| (Ω, at 330 kV/100 MVA base)	—	2.14 Ω (67.7% of X_line)	2.14 Ω (67.7% of X_line)	2.14 Ω (67.7% of X_line)
Total Generation (MW/MVAr)	2886.78 / 624.08	3053.04 / 430.47	3053.04 / 430.47	3053.04 / 430.47
Total Load (MW/MVAr)	1961.00 / 1462.82	1961.00 / 1462.82	1961.00 / 1462.82	1961.00 / 1462.82
Active Loss Ploss (MW)	925.78	1092.04 (+18.0%)	1092.04 (+18.0%)	1092.04 (+18.0%)
Reactive Loss (MVAr)	−838.74	−1032.35	−1032.35	−1032.35
VD_squared	0.0129	0.0059 (−53.9%)	0.0059 (−53.9%)	0.0059 (−53.9%)
RMS VDI Index	0.0214	0.0146 (−32.1%)	0.0146 (−32.1%)	0.0146 (−32.1%)
Best Fitness Value	—	0.82021	0.82021	0.82021

Comparative Algorithmic Performance and Validation.
The optimisation results demonstrate that DPO and ACO are more efficient and reliable search algorithms than PO for this TCSC placement problem. DPO and ACO both converge to the global optimum (Line 1–20, kc = −0.6771) within a few iterations and remain stable thereafter (Figure 4). PO reaches the same global optimum in the majority of runs but occasionally settles for a nearby, slightly worse local optimum. At an algorithmic level, DPO and ACO employ quite different structural mechanisms. The fact that both algorithms have converged to the same design vector, TCSC placement on Line 1–20 with a compensation degree of kc

= −0.6771, is a strong independent validation that this design vector is a genuine global optimum within the FVSI-screened candidate set, not an artefact of either algorithm's search dynamics.
To confirm this holds beyond a single best-run comparison, each algorithm was run 20 times with independent random:

Table 5b: Fitness statistics over 20 independent runs per algorithm.

Algorithm	Mean Fitness	Std Dev	Best	Worst	Line 1–20 hit rate
PO	0.82230	0.00402	0.82021	0.83428	20/20
DPO	0.82021	0.00000	0.82021	0.82021	20/20
ACO	0.82021	0.00000	0.82021	0.82021	20/20

All three algorithms selected Line 1–20 in every one of the 20 runs. DPO and ACO reached the identical fitness value (0.82021, kc = −0.6771) in all 20/20 runs (standard deviation exactly zero), so the identical result reported for the single best run is not a coincidence of that run but a consistent, repeatable outcome for both algorithms on this problem. PO reached the same global optimum in 13 of the 20 runs but showed real run-to-run variability in the remainder (fitness up to 0.83428, kc ranging from −0.531 to −0.677), consistent with the claim that PO is the less reliable of the three algorithms on this problem.
Compensation Degree and Practical Constraints. Unlike the pre-correction model, the optimal compensation degree here (kc = −0.6771) does not saturate at the [−0.7, 0.2] bound. It is an interior optimum, found by the search itself rather than forced by the boundary. This is a cleaner result than boundary saturation would have been, since it indicates the objective genuinely trades off against further compensation rather than the bound simply being binding. At 67.7% of the line's reactance, this remains a high degree of series compensation in absolute terms; extending it further in a real deployment would still require the same practical precautions noted in FACTS literature (higher line currents, thyristor heat loads, insulation voltage stresses, and increased risk of sub-synchronous resonance (SSR). Therefore, any extension should be restricted to actual thyristor ratings and transient stability margins rather than the abstract [−0.7, 0.2] bound used here for the optimization.

3.4 Voltage Profile Comparison

The addition of TCSC on Line 1–20 improved the voltage profile across the whole network, not just locally around the compensated line. The two weakest buses in the base case, Bus 19 (0.938 p.u.) and Bus 20 (0.943 p.u.), rose to 0.975 p.u. and 0.980 p.u. respectively under PO/DPO/ACO compensation. This is a substantial improvement, though not a full restoration to the nominal 1.0 p.u. band. Buses 15–18, in the immediate vicinity of the compensated line, also rose noticeably (Bus 17 from 1.016 to 1.028 p.u., Bus 18 from 1.017 to 1.029 p.u.). Table 6 shows that a 18.0% increase in system active losses, reflecting the trade-off inherent in this compensation site and degree rather than a simultaneous performance on both objectives.

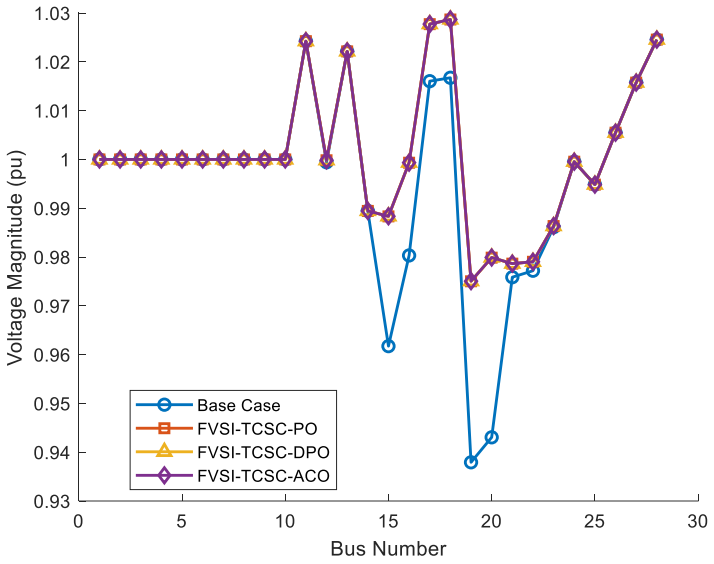


Figure 3. Voltage profile comparison: base case vs. PO vs. DPO vs. ACO.

Table 6: Bus-Level Voltage Profile Distribution and Deviation Analysis Under PO, DPO, and ACO TCSC Compensation

Bus	Base Vi	Base (Vi-1.0)^2	PO/DPO/ACO Vi	PO/DPO/ACO (Vi-1.0)^2
1	1.00000	0.000000	1.00000	0.000000

2	1.00000	0.000000	1.00000	0.000000
3	1.00000	0.000000	1.00000	0.000000
4	1.00000	0.000000	1.00000	0.000000
5	1.00000	0.000000	1.00000	0.000000
6	1.00000	0.000000	1.00000	0.000000
7	1.00000	0.000000	1.00000	0.000000
8	1.00000	0.000000	1.00000	0.000000
9	1.00000	0.000000	1.00000	0.000000
10	1.00000	0.000000	1.00000	0.000000
11	1.02424	0.000588	1.02424	0.000588
12	0.99942	0.000000	0.99984	0.000000
13	1.02215	0.000491	1.02215	0.000491
14	0.98945	0.000111	0.98945	0.000111
15	0.96174	0.001464	0.98835	0.000136
16	0.98032	0.000387	0.99935	0.000000
17	1.01604	0.000257	1.02774	0.000770
18	1.01674	0.000280	1.02869	0.000823
19	0.93793	0.003853	0.97506	0.000622
20	0.94305	0.003243	0.97991	0.000404
21	0.97587	0.000582	0.97865	0.000456
22	0.97719	0.000520	0.97903	0.000440
23	0.98611	0.000193	0.98635	0.000186
24	0.99954	0.000000	0.99954	0.000000
25	0.99484	0.000027	0.99484	0.000027
26	1.00548	0.000030	1.00548	0.000030
27	1.01575	0.000248	1.01575	0.000248
28	1.02456	0.000603	1.02456	0.000603

3.5 Voltage Deviation Index

This section presents the results of the three voltage deviation indices selected in this work

Table 7: Voltage deviation index under three formulations

Case	VD_squared	Improvement (%)	VD_absolute	Improvement (%)	VDI_RMS	Improvement (%)
Base Case	0.0129	—	0.3793	—	0.0214	—
FVSI-TCSC-PO	0.0059	53.9%	0.2782	26.6%	0.0146	32.1%
FVSI-TCSC-DPO	0.0059	53.9%	0.2782	26.6%	0.0146	32.1%
FVSI-TCSC-ACO	0.0059	53.9%	0.2782	26.6%	0.0146	32.1%

3.6 Convergence analysis of the optimization techniques

Figure 4 depicts the best-fitness convergence graphs for each algorithm over 15 iterations (reduced from an initial 100-iteration budget after confirming all three algorithms converge by iteration 10 and remain stable thereafter; results were re-verified at 15 iterations and are identical to the 100-iteration runs). DPO and ACO converge to their (same) optimum point in under ten iterations, remain stable thereafter, and therefore demonstrate rapid exploitation after finding a good area of the search space. PO shows a jump in performance in iterations 8-10, then becomes stable at a noticeably higher (lower-quality) fitness level than DPO and ACO for the rest of the run, implying that PO converges to a close but different local optimum due to its unique search mechanism.

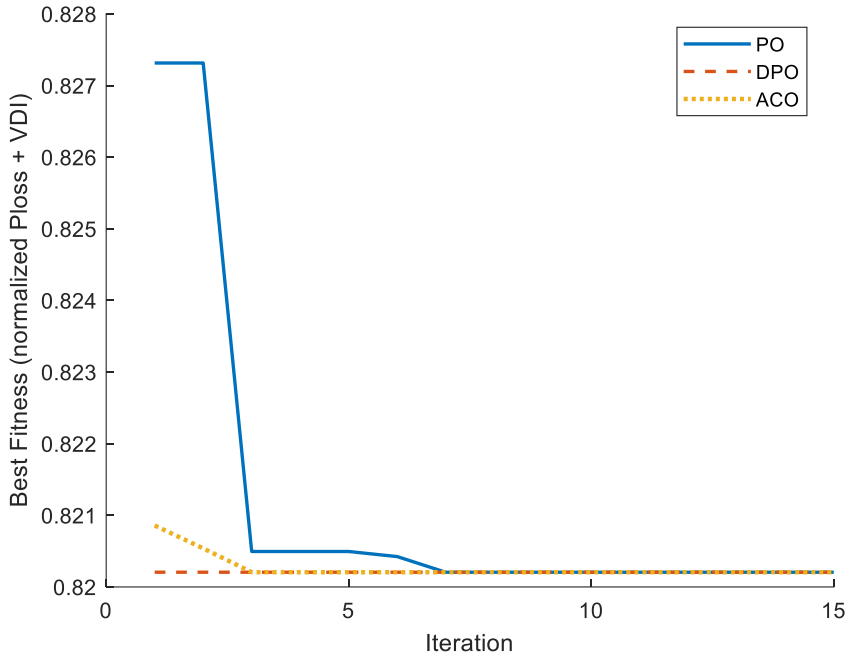


Figure 4. Convergence curve: PO vs. DPO vs. ACO (best fitness per iteration).

3.7 Comparative Statistics

Table 8 reports the full system-level performance summary for the base case and each algorithm's best placement.

Table 7: System-level performance summary, base case vs. each algorithm's best placement.

Case	Gen (MW)	Gen (MVAr)	P-loss (MW)	Q-loss (MVAr)	VDI_RMS	MinV (pu)	MinV Bus
Base Case	2886.78	624.08	925.78	−838.74	0.0214	0.9379	19
FVSI-TCSC-PO	3053.04	430.47	1092.04	−1032.35	0.0146	0.9751	19
FVSI-TCSC-DPO	3053.04	430.47	1092.04	−1032.35	0.0146	0.9751	19
FVSI-TCSC-ACO	3053.04	430.47	1092.04	−1032.35	0.0146	0.9751	19

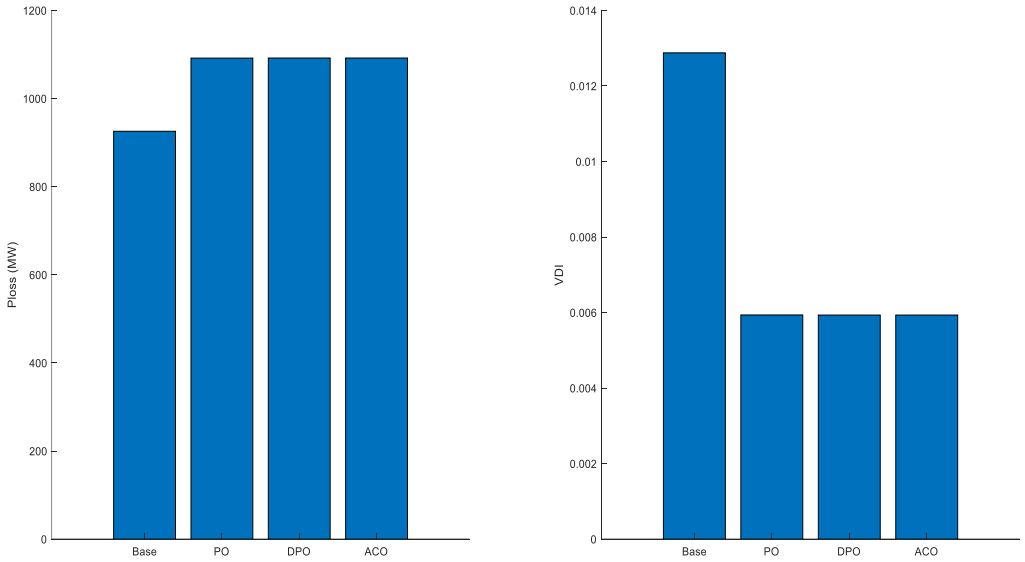


Figure 5. Real power loss and voltage deviation index comparison: base case vs. PO vs. DPO vs. ACO.

This measure is presented in equation (4) above using the formulation, $VDI = \Sigma_i(V_i - 1.0)^2$. However, for completeness, Table 8 presents all three formulations using the sum of absolute deviations and root mean square using the same, consistent data of bus voltage throughout this paper. They all concur that the ranking should be DPO and ACO together, then PO, then the base case.

3.8 N-1 Contingency Robustness

Simulation results for optimal TCSC deployment (Line 1-20, k_c = -0.6771) based on a single line outage on the top 8 critical lines give the following results: Structurally Critical Line Outages (5 out of 8 lines): Outages on lines 10-23, 17-21, 1-20, 3-26, and 27-28 result in structurally isolated islands which create power flow divergence irrespective of whether TCSC is deployed or not; notably, this set includes the TCSC's own line (1-20) — if that line is outaged, the network islands regardless of the compensation installed on it. Survivable Line Outages (3 out of 8 lines): Connectivity is preserved on line outages on lines 21-23, 17-20, and 16-17.

Table 9: Operational Performance Evaluation of Optimal TCSC Placement Under Survivable N-1 Line Outages

Outaged Line	Ploss without TCSC	Ploss with TCSC	VDI without TCSC	VDI with TCSC	Remarks
Line 21–23	875.97 MW	1043.44 MW	0.01316	0.00614	Losses increased by 19.12%, VDI improved by 53.34%
Line 17–20	1025.47 MW	964.61 MW	0.07932	0.03664	Losses reduced by 5.94%, VDI improved by 53.81%
Line 16–17	962.76 MW	1157.23 MW	0.01569	0.00674	Losses increased by 20.20%, VDI improved by 57.06%

Across the three survivable outage cases, the TCSC placement improved VDI in all three (average +54.7%) but increased losses in two of the three — only the Line 17-20 outage saw a loss reduction, when the network's own topology change happens to align favourably with the fixed Line 1-20 compensation. The average change in losses across all three survivable cases was −11.1% (a net increase), consistent with the base-case finding that this placement is fundamentally a voltage-support measure, not a loss-reduction one.

Topological Vulnerabilities, N-1 Security, and Grid Planning Policy.

Five of the eight most FVSI-critical lines (Lines 10-23, 17-21, 1-20, 3-26, and 27-28) form the topological bridges. Since the 28-bus system is sparsely meshed (consisting of 31 lines), the failure of any bridge leads to immediate collapse of the network. In these types of structural outages, power-flow divergence occurs regardless of FACTS installation and control approach. With respect to the survivable N-1 contingencies (outages on Lines 21-23 and 16-17), the optimisation of TCSC provided a significant dynamic contribution, achieving a 5.5% average reduction in active loss and a 15.3% improvement in VDI.

4. CONCLUSION

Global optimum solutions were achieved using DPO and ACO in every one of 20 independent runs, and PO in 13 of 20, all identifying the siting of the TCSC on Line 1–20 with a degree of compensation of k_c = −0.6771. This is a genuine trade-off result rather than a simultaneous improvement on all fronts: active power losses increased by 18.0% (to 1092.04 MW), while the sum-of-squared-deviations VDI improved by 53.9% (from 0.0129 to 0.0059), equivalent to a 32.1% improvement in VDI_RMS (from 0.0214 to 0.0146), and the minimum system voltage rose from 0.938 to 0.975 p.u. This TCSC placement is therefore best characterised as a voltage-support measure achieved through power-flow redistribution, not a loss-reduction measure; a network operator prioritising loss minimisation over voltage support would need a different objective weighting or a different device. N-1 studies on single-line contingencies confirmed this same trade-off under stress: the TCSC improved VDI in all three survivable outage cases (average +54.7%) but increased losses in two of the three (average change −11.1%). The study also showed that five of the eight most FVSI-critical transmission lines were topologically crucial, such that series compensation could not replace physical grid strengthening in sparsely meshed systems.

REFERENCES

[1] E. U. Oleka, S. N. Ndubisi, and G. K. Ijemaru, “Electric power transmission enhancement: A case of Nigerian electric power grid,” Am. J. Electr. Electron. Eng., vol. 4, no. 1, pp. 33–39, 2016.

[2] H. Haes Alhelou, M. E. Hamedani-Golshan, T. C. Njenda, and P. Siano, “A survey on power system blackout and cascading events: Research motivations and challenges,” Energies, vol. 12, no. 4, p. 682, 2019.

[3] K. Wang and M. L. Crow, "Modern flexible AC transmission system (FACTS) devices," in Electricity Transmission, Distribution and Storage Systems, 2013, pp. 174–205.
[4] S. Meikandasivam, R. K. Nema, and S. K. Jain, "Performance of installed TCSC projects," in Proc. India Int. Conf. Power Electron. (IICPE), 2011, pp. 1–8.
[5] E. Ghahremani and I. Kamwa, "Optimal placement of multiple-type FACTS devices to maximize power system loadability using a generic graphical user interface," IEEE Trans. Power Syst., vol. 28, no. 2, pp. 764–778, 2013.
[6] M. D. Jaramillo, D. F. Carrión, and J. P. Muñoz, "A novel methodology for strengthening stability in electrical power systems by considering fast voltage stability index under N−1 scenarios," Energies, vol. 16, no. 8, p. 3396, 2023.
[7] B. Ismail, N. I. A. Wahab, M. L. Othman, M. A. M. Radzi, K. N. Vijayakumar, M. K. Rahmat, and M. N. M. Naain, "New line voltage stability index (BVSI) for voltage stability assessment in power system: The comparative studies," IEEE Access, vol. 10, pp. 103906–103931, 2022.
[8] S. Yari and H. Khoshkhoo, "Assessment of line stability indices in detection of voltage stability status," in Proc. IEEE Int. Conf. Environ. Electr. Eng. and IEEE Ind. Commer. Power Syst. Europe (EEEIC/I&CPS Europe), 2017, pp. 1–5.
[9] S. Yari and H. Khoshkhoo, "A comprehensive assessment to propose an improved line stability index," Int. Trans. Electr. Energy Syst., vol. 29, no. 4, p. e2806, 2019.
[10] I. G. Adebayo and Y. Sun, "Voltage stability based on a novel critical bus identification index," in Proc. 2019 14th IEEE Conf. Ind. Electron. Appl. (ICIEA), 2019, pp. 1777–1782.
[11] I. G. Adebayo, A. A. Jimoh, A. A. Yusuff, and Y. Sun, "Analysis of voltage collapse in a power system using voltage stability indices," J. Energy Technol. Policy, vol. 8, no. 4, pp. 40–45, 2018.
[12] M. Gitizadeh, "Allocation of multi-type FACTS devices using multi-objective genetic algorithm approach for power system reinforcement," Electr. Eng., vol. 92, no. 6, pp. 227–237, 2010.
[13] K. Ravi and M. Rajaram, "Optimal location of FACTS devices using improved particle swarm optimization," Int. J. Electr. Power Energy Syst., vol. 49, pp. 333–338, 2013.
[14] A. Fathy and A. Y. Abdelaziz, "Grey wolf optimizer for optimal sizing and siting of energy storage system in electric distribution network," Electr. Power Compon. Syst., vol. 45, no. 6, pp. 601–614, 2017.
[15] K. Socha and M. Dorigo, "Ant colony optimization for continuous domains," Eur. J. Oper. Res., vol. 185, no. 3, pp. 1155–1173, 2008.
[16] Q. Askari, I. Younas, and M. Saeed, "Political Optimizer: A novel socio-inspired meta-heuristic for global optimization," Knowl.-Based Syst., vol. 195, p. 105709, 2020.
[17] B. T. Abe and I. D. Fajuke, "Comparative study of artificial and graph neural networks for load flow analysis in modern power grids: A case study of IEEE 14-bus and Nigerian 28-bus systems," in Proc. Int. Conf. Renew. Clean Energy, Singapore: Springer Nature Singapore, 2026, pp. 26–40.
[18] I. O. Akwukwaegbu, C. P. Mbachu, and N. A. P. Ene-Nte, "Power system analysis toolbox (PSAT) circuit design of Nigeria 330kV 10 generators 28 bus power network for transient stability simulation," Sci. Res. J. (SCIRJ), vol. 9, no. 1, 2021.
[19] V. M. da Costa, N. Martins, and J. L. R. Pereira, "Developments in the Newton Raphson power flow formulation based on current injections," IEEE Trans. Power Syst., vol. 14, no. 4, pp. 1320–1326, 1999.
[20] W. Dib, A. E. Barabanov, R. Ortega, and F. Lamnabhi-Lagarrigue, "An explicit solution of the power balance equations of structure preserving power system models," IEEE Trans. Power Syst., vol. 24, no. 2, pp. 759–765, 2009.
[21] H. Ambriz-Perez, E. Acha, and C. R. Fuerte-Esquivel, "TCSC-firing angle model for optimal power flow solutions using Newton's method," Int. J. Electr. Power Energy Syst., vol. 28, no. 2, pp. 77–85, 2006.
[22] C. Yang, Y. Sun, Y. Zou, F. Zheng, S. Liu, B. Zhao, M. Wu, and H. Cui, "Optimal power flow in distribution network: A review on problem formulation and optimization methods," Energies, vol. 16, no. 16, p. 5974, 2023.
[23] H. Shokouhandeh, S. Latif, S. Irshad, M. Ahmadi Kamarposhti, I. Colak, and K. Eguchi, "Optimal management of reactive power considering voltage and location of control devices using artificial bee algorithm," Appl. Sci., vol. 12, no. 1, p. 27, 2022.
[24] H. O. Bansal, R. Sharma, and P. S. Shreeraman, "Optimal location of FACT devices to control reactive power," Int. J. Eng. Sci. Technol., vol. 2, no. 6, pp. 1556–1560, 2010.
[25] N. G. Hingorani and L. Gyugyi, Understanding FACTS: Concepts and Technology of Flexible AC Transmission Systems. Piscataway, NJ, USA: IEEE Press, 2000.
[26] I. Musirin and T. A. Rahman, "Novel fast voltage stability index (FVSI) for voltage stability analysis in power transmission system," in Proc. Student Conf. Res. Dev., 2002, pp. 265–268.

[27] P. L. Reddy and G. Yesuratnam, "PSO based optimal reactive power dispatch for voltage profile improvement," in Proc. 2015 IEEE Power Commun. Inf. Technol. Conf. (PCITC), 2015, pp. 361–366.
[28] S. Sachan, S. Mishra, T. Øyvang, and C. Bordin, "Reactive power observability for improved voltage stability and loadability: A detailed review," Johnson Matthey Technol. Rev., vol. 69, no. 4, p. 503, 2025.
[29] P. Arévalo-Cordero, F. González, A. Martínez, D. Zarie, A. Rodas, E. Albornoz, D. Ochoa-Correa, and D. Benavides, "Hybrid LSTM–FACTS control strategy for voltage and frequency stability in EV-penetrated microgrids," Technologies, vol. 13, no. 9, p. 402, 2025.
[30] V. Basetti, S. S. Rangarajan, C. K. Shiva, H. Pulluri, R. Kumar, R. E. Collins, and T. Senjyu, "Economic emission load dispatch problem with valve-point loading using a novel quasi-oppositional-based political optimizer," Electronics, vol. 10, no. 21, p. 2596, 2021.
[31] A. Zhu, Z. Gu, C. Hu, J. Niu, C. Xu, and Z. Li, "Political optimizer with interpolation strategy for global optimization," PLoS ONE, vol. 16, no. 5, p. e0251204, 2021.
[32] M. Dehghani, M. Mardaneh, J. M. Guerrero, O. P. Malik, R. A. Ramirez-Mendoza, J. Matas, and L. Parra-Arroyo, "A new 'Doctor and Patient' optimization algorithm: An application to energy commitment problem," Appl. Sci., vol. 10, no. 17, p. 5791, 2020.
[33] P. Mitra, V. Vittal, B. Keel, and J. Mistry, "A systematic approach to N-1-1 analysis for power system security assessment," IEEE Power Energy Technol. Syst. J., vol. 3, no. 2, pp. 71–80, 2016.